VOL. 11, NO. 23, DECEMBER 2016 ISSN 1819-6608
ARPN Journal of Engineering and Applied Sciences

www.arpnjournals.com

POWER CONTROL OF DFIG BASED WIND SYSTEM: COMPARISON BETWEEN ACTIVE DISTURBANCE REJECTION CONTROLLER AND PI CONTROLLER

Choroq Z. El Archi[1], Tamou Nasser[2] and Ahmed Essadki[1]
[1]Normal Superior School of Technical Education, University of Mohammed V - Rabat, Morocco
[2]National School of Computer Science and Systems Analysis, University of Mohammed V, Rabat, Morocco
E-Mail: elarchichoroq@gmail.com

ABSTRACT

Since the wind speed is random and unpredictable, the control of the power flowing between the wind energy conversion system (WECS) and the electric grid is challenging. In this paper, the active disturbance rejection controller (ADRC) and the PI controller are used in the control of a variable speed wind system based on the doubly fed induction generator (DFIG). This generator is controlled via its rotor which is connected to the grid by two back to back converters, a DC bus and a filter. For the rotor side converter (RSC), the voltage reference is provided by the rotor current control loop. This control loop gets its reference from the maximum power point tracking (MPPT) algorithm used to maximize the power extracted from the wind. As for the grid side converter (GSC), its voltage reference is obtained from the DC voltage regulation. All is simulated in Matlab/Simulink environment and both controllers are compared in terms of reference tracking and robustness against parametric variations. Results show that ADRC drives the system to its reference quicker than the PI with no weakness to modeling errors or parametric variations and with respect to the desired time response. In addition, the test results proved a high sensitivity of the PI controller to parametric variations.

Keywords: wind energy, DFIG, PI controller, ADRC, parametric variation.

INTRODUCTION

Electricity has become very important in our life. Every day people use a lot of electrical and electronic devices that are crucial in the modern society and for people's well being. This electrical energy we use comes mainly from fossil fuels. Unluckily, these sources of energy are causing our planet to heat up due to greenhouse gases produced in the process of fossil fuels combustion. So, with no measures taken, the annual global emission of greenhouse gases that would result in 2030 is likely to be 68 billion tons of carbon-dioxide-equivalent [1]. This number is "far higher than an emission pathway that would be consistent with having 50 to 66 percent chance of avoiding global warming of more than 2°C" [1]. And for that, according to the outcome of the 21st conference of parties (COP21) held in Paris, the global emission of greenhouse gases should be 55 billion of carbon-dioxide-equivalent by 2030 rather than 68 billion. Moreover, the continuous increase of the electrical demand is exhausting our planet reserve of the fossil fuels. And that too, is another reason to make us look for alternative resources that would provide us and the coming generations with the needed energy.

In the light of this decision, all countries should be able to insure 40% of their energy from renewable sources by 2030 and 50% by 2040. As for our country, Morocco promised to achieve the same results ten years earlier [2]. Among these renewable sources, there is the wind energy which has a lot of project in process in Morocco. That is why there is a lot of interest and attention paid to the research in the control of wind systems.

In the present work, we are interested in the electrical part of the research which is mainly about the control of the power flowing between the generator of WECS and the power grid. In fact, there are different types of WECS configurations using different types of generators. But, this work is held on a variable speed WECS based on the doubly fed induction generator. It's the most dominant configuration with half the market share [3] [4]. Compared to full variable speed WECS based on the permanent magnet synchronous generator (PMSG) in which the power converter are sized for 100% of the rated power, the DFIG based system is less expensive because its power converters are only sized for 30% of the rated power.

The generator in a DFIG based system is connected to the grid via both the stator and the rotor. The stator is directly connected to the grid while the rotor is separated from the grid by back to back converters, a DC link and a filter. It can operate in two modes; the subsynchronous and the super synchronous mode. During the first mode, the rotor consumes power from the grid while in the second mode, both the rotor and the stator produce energy and send it to the power grid.

The first section of this paper is dedicated to the modeling of the different parts of the wind system such as the wind turbine, the generator, the power converters, the DC link and the RL filter. The second section is dedicated to the presentation, the synthesizing and the application of the PI controller and the ADRC in the different control loops in the system. Finally, the last section in about testing the controllers and comparing the simulation results.

MODELING THE WIND ENERGY SYSTEM

Modeling the wind turbine

The turbine consists of three blades, a nacelle, a gear box and a generator mounted on a tour. By applying the fundamental law of dynamics on the generator rotor, we evaluate the evolution of the generator rotational speed Ω_{gen} as in Equation (1) [5].

$$J.\frac{d\Omega_{\text{gen}}}{dt} = C_g + f.\Omega_{gen} - C_{em} \quad (1)$$

J is the moment of inertia of the hole system on the rotor axis, C_{em} is the electromagnetic torque produced by the generator, C_g is the mechanical torque applied on the rotor after the gearbox, and f is the coefficient of the viscous frictions.

Equation (2) is an application of Laplace transformation to Equation (1).

$$\Omega_{gen} = \frac{1}{J.s+f}.(C_g - C_{em}) \quad (2)$$

Computation of C_g

Betz showed that a wind turbine can't convert more than 59 per cent of the kinetic energy it receives from the wind into mechanical energy [6]. This percentage is given for every wind turbine by its manufacturer and is called the power coefficient (Cp). The extractible power is then equal to the total power available in the wind (P_t) multiplied by Cp. P_t is given by Equation (3) [7].

$$P_t = \frac{\rho.S.V^3}{2} \quad (3)$$

V is the wind speed, ρ is the air density, and S is the area swept by the turbine blades.
From above, Cg can be given by Equation (4).

$$C_g = \frac{1}{2}.C_p.\rho.S.V^3.\frac{1}{\Omega_{tur}}.\frac{1}{G} = \frac{1}{2}.C_p.\rho.\pi.R^3.V^2.\frac{1}{\lambda}.\frac{1}{G} \quad (4)$$

G is the coefficient of the gearbox, R is the length of the turbine blades, $\Omega_{tur}$is the turbine rotational speed, λ is the tip speed ratio given by Equation (5).

$$\lambda = \frac{\Omega_{tur}.R}{V} \quad (5)$$

The Cp used in this work is the power coefficient of the 1.5 MW DFIG based wind system adopted in the wind turbine model of Matlab/Simulink, it is given in Equation (6).

$$C_p(\lambda,\beta) = c_1.\left(\frac{c_2}{\lambda_i} - c_3.\beta - c_4\right).e^{\frac{c_5}{\lambda_i}} + c_6.\lambda \quad (6)$$

β is the pitch angle and λ_i is as in Equation (7).

$$\frac{1}{\lambda_i} = \frac{1}{\lambda+0{,}08.\beta} - \frac{0{,}035}{\beta^3+1} \quad (7)$$

Computation of C_{em}

As for C_{em}, we used a maximum power point tracking algorithm that is without speed control and relies on the fact that C_{em} is equal to its referential value gotten from Equation (4) [8]. This C_{em_ref} is given in Equation (8).

$$C_{em\_ref} = \frac{1}{2}.C_{p\_max}.\rho.\pi.R^5.\frac{\Omega_{gen}^2}{(G.\lambda_{Cp\_max})^3} \quad (8)$$

Figure-1 presents the curve of the power coefficient in term of the tip speed ratio λ, for different values of the pitch angle β.

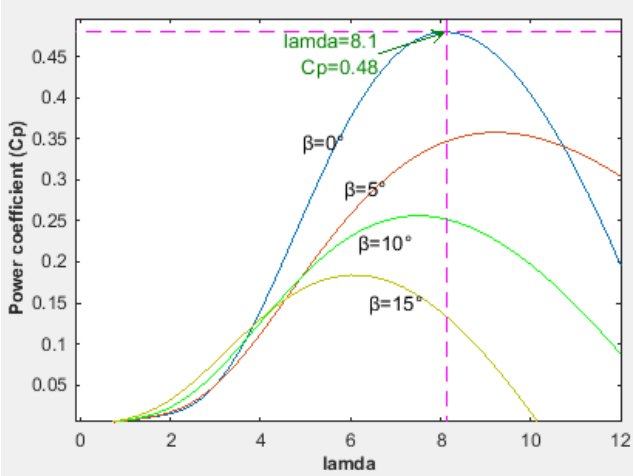

Figure-1. Power coefficient of the wind turbine in term of Lamda.

Modeling the DFIG

The two phase model of the DFIG is giving in Equation (9) to (13) [9].

$$\begin{cases} V_{sd} = R_s.i_{sd} + \frac{d\varphi_{sd}}{dt} - \omega_s.\varphi_{sq} \\ V_{sq} = R_s.i_{sq} + \frac{d\varphi_{sq}}{dt} + \omega_s.\varphi_{sd} \\ V_{rd} = R_r.i_{rd} + \frac{d\varphi_{rd}}{dt} - \omega_r.\varphi_{rq} \\ V_{rq} = R_r.i_{rq} + \frac{d\varphi_{rq}}{dt} + \omega_r\varphi_{rd} \end{cases} \quad (9)$$

$$\begin{cases} \varphi_{sd} = L_s.i_{sd} + M.i_{rd} \\ \varphi_{sq} = L_s.i_{sq} + M.i_{rq} \\ \varphi_{rd} = L_r.i_{rd} + M.i_{sd} \\ \varphi_{rq} = L_r.i_{rq} + M.i_{sq} \end{cases} \quad (10)$$

$$\begin{cases} P_s = V_{sd}.i_{sd} + V_{sq}.i_{sq} \\ Q_s = V_{sq}.i_{sd} - V_{sd}.i_{sq} \end{cases} \quad (11)$$

$$\begin{cases} P_r = V_{rd}.i_{rd} + V_{rq}.i_{rq} \\ Q_r = V_{rq}.i_{rd} - V_{rd}.i_{rq} \end{cases} \quad (12)$$

$$C_{em} = -P.\frac{M}{L_s}.(i_{rd}.\varphi_{sq} + i_{rq}.\varphi_{sd}) \quad (13)$$

Considering that the generator is unsaturated and the d axis of the two phase reference is oriented along the stator flux vector to ensure decoupling between the stator and the rotor in the electromagnetic torque expression, the DFIG can be presented by the new simplified model in Eq.(14) to (17), and Figure-2.

$$i_{rd} = \frac{1}{R_r + s.\left(L_r - \frac{M^2}{L_s}\right)}.\left(V_{rd} + \omega_r.\left(L_r - \frac{M^2}{L_s}\right).i_{rq}\right) \quad (14)$$

$$i_{rq} = \frac{1}{R_r + s.\left(L_r - \frac{M^2}{L_s}\right)}.\left(V_{rq} - \omega_r.\left(L_r - \frac{M^2}{L_s}\right).i_{rd} - \frac{\omega_r}{\omega_s}.\frac{M}{L_s}.V_s\right) \quad (15)$$

$$\begin{cases} P_s = V_s.-\frac{M}{L_s}.i_{rq} \\ Q_s = V_s.\frac{\varphi_s - M.i_{rd}}{L_s} \end{cases} \quad (16)$$

$$C_{em} = -P.\frac{M}{L_s}.\frac{V_s}{\omega_s}i_{rq} \quad (17)$$

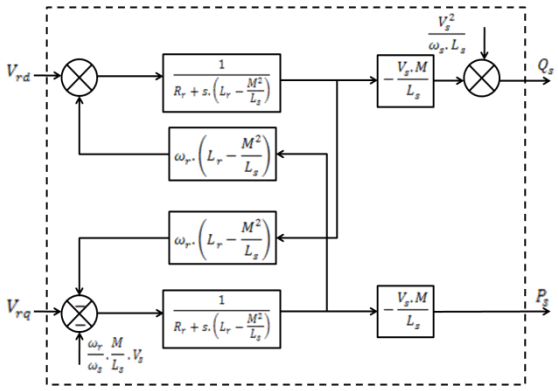

Figure-2. Model of the DFIG in dq synchronous reference.

With the reference value of the electromagnetic torque given in Equation (8), we get the reference value of the quadratic rotor current. As for the direct rotor current, it's deduced from the desired value of the reactive power in Equation (16). The results are given in Equation (18).

$$\begin{cases} i_{rq\_ref} = -\frac{2}{3}.\frac{L_s.\omega_s}{V_s.M.P}.C_{em\_ref} \\ i_{rd\_ref} = \left(\frac{V_s}{\omega_s} - \frac{2}{3}.Q_{s\_ref}\frac{.L_s}{V_s}\right).\frac{1}{M} \end{cases} \quad (18)$$

Modeling The PWM Converters, The RL Filter and DC link.

Figure-3 presents the PWM converters and the RL filter in the rotor /grid connection.

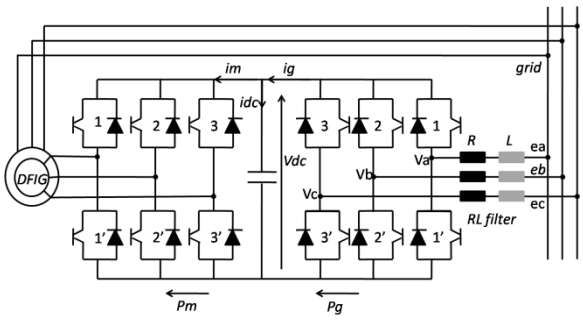

Figure-3. The PWM converter, DC link, and the RL filter.

PWM converter

The truth table and the Karnaugh maps of all possible sequences of the six switches of a PWM converter are established to get the expression of each phase voltage of the AC side. Example of Karnaugh map is given in Table-1 for the voltage between a and phase b. Expressions of all voltage are then given in Equation (19) [10].

Table-1. Karnaugh Map for voltage between two phases (e.g. V_{ab}).

S_bS_c / S_a	00	01	11	10
0	0	0	- V_{dc}	- V_{dc}
1	V_{dc}	V_{dc}	0	0

$$\begin{cases} V_a = \frac{(2S_a - S_b - S_c)}{3}.V_{dc} \\ V_b = \frac{(2S_b - S_a - S_c)}{3}.V_{dc} \\ V_c = \frac{(2S_c - S_a - S_b)}{3}.V_{dc} \end{cases} \quad (19)$$

The current in the DC side of the converter depends on the states of the switches and the AC current in the AC side of the converter. e.g. the current in the dc side of the RSC is given by equation (20).

$$i_m = S_1 i_1 + S_2 i_2 + S_3 i_3 \quad (20)$$

V_{dc} is the voltage in the DC link, S_k is the state of the switch referred to by k, and i_k is the current in the phase k of the rotor.

RL filter

The three phase model of the RL filter is deduced from Figure-3.

$$\begin{cases} e_a - V_a = (L.s + R).i_a \\ e_b - V_b = (L.s + R).i_b \\ e_c - V_c = (L.s + R).i_c \end{cases} \quad (21)$$

Equation (22) is the result of Park transformation applied to previous Equation (21) to get dq model of the RL filter [8].

$$\begin{cases} i_{fd} = \frac{1}{R+L.s}.(V_{fd} - e_d + L.\omega_s.i_q) \\ i_{fq} = \frac{1}{R+L.s}.(V_{fq} - e_q - L.\omega_s.i_d) \end{cases} \quad (22)$$

DC Link

The capacitor consisting the DC link is connecting the grid side converter to the rotor side converter as in Figure-3. As given in Equation (23), the energy W stored in this capacitor depends on both Pm and Pg that are respectively the power consumed by the rotor and the power received from the grid [11].

$$\frac{dW}{dt} = C.V_{dc}.\frac{dV_{dc}}{dt} = P_g - P_m \quad (23)$$

with

$$P_g = V_{dc}.i_g \text{ and } P_m = V_{dc}.i_m \quad (24)$$

i_m refers to the current flowing from the DC link of the RSC and i_g refers to the current flowing from the GSC to the DC link.

If we neglect the losses in the converter and the filter, we get that the power flowing through the filter and GSC is the same as the power absorbed from the grid noted P_f Equation (28).

$$P_g = P_f = V_d.i_d + V_q.i_q = V_q.i_q \quad (25)$$

$V_{d,q}$ and $I_{d,q}$ are the space vectors of the voltage and current in the AC side of the GSC.

Also, with the triangulo-sinusoidal pulse width modulation (PWM), the maximum sinusoidal amplitude reference is $\frac{V_{dc}}{2}$ [12]. Therefore, the output phase peak of the AC voltage of the converter, referred to by V_{conv} and its representation in dq reference V_q are as follows [13]:

$$V_{conv} = ma.\frac{V_{dc}}{2} \quad (26)$$

$$V_q = -ma.\sqrt{\frac{3}{2}}.\frac{V_{dc}}{2} \quad (27)$$

ma is the modulation amplitude ratio of the sinusoidal PWM.

From Equation (26), (27) and (28), we deduce that:

$$i_g = -\frac{ma.\sqrt{3}}{2.\sqrt{2}}.i_q \quad (28)$$

Finally, the dq model of the DC link is given by Equation (29).

$$V_{dc} = -\frac{ma.\sqrt{3}}{s.C.2.\sqrt{2}}.i_q - \frac{1}{s.C}.i_m \quad (29)$$

CONTROL OF THE DFIG

PI controller

The transfer function of the proportional integral controller is:

$$PI(s) = K_p + \frac{K_i}{s} \quad (30)$$

In order to identify the parameters K_p and K_i of the PI controllers used in the system, different methods are employed. For the control of direct and quadratic rotor and grid currents, the method of pole compensation is used and the results are given in Equation (31) and Equation (32) [9]. For the DC bus voltage regulation, the system is a pure integrator that should be easily controlled by a proportional controller. But with the presence of a disturbance upstream of the system, an additional integrator becomes mandatory to overcome the residual steady sate error known as the offset. As a result, K_p and K_i are chosen as presented in Equation (33)

$$PI_r(s) = \frac{\left(L_r - \frac{M^2}{L_s}\right)}{\tau_r} + \frac{R_r}{\tau_r}.\frac{1}{s} \quad (31)$$

$$PI_r(s) = \frac{L_f}{\tau_r} + \frac{R_f}{\tau_r}.\frac{1}{s} \quad (32)$$

τ_r is the time response desired for rotor currents.

$$\begin{cases} \frac{K_i}{K_p} \ll \frac{\omega_c}{10} \\ \left|\left(K_p + \frac{K_i}{s}\right).\frac{ma.\sqrt{3}}{s.C.2.\sqrt{2}}\right| = 1 \end{cases} \quad (33)$$

ω_c is the cutoff frequency of the open loop system.

ADRC

ADRC on a first order system

To introduce the Active disturbance rejection control (ADRC) suggested by Han in 1995 [14], we consider a first order system with a single-input (u), a single-output (y), and a disturbance (f) as in Equation (34) [14] [15] [16].

$$\begin{cases} \dot{x_1} = f(x_1, d(t), t) + bo.u(t) \\ y = x_1 \end{cases} \quad (34)$$

$f(x_1, d(t), t)$ is the total disturbance. It's a multivariable function of the state variable, the internal model of the plant, and the external disturbances on the input signal. This function must be totally estimated and rejected to make the system converge to the desired reference via the control signal. To insure that, Han saw that the total disturbance should be considered as an additional state variable to be estimated by an observer he named the extended state observer (ESO). With this extension, the system in Equation (34) becomes as in Equation (35) and Equation (36). Also, the ESO is a Leumberger observer given in Equation (37).

$$\begin{cases} \dot{x_1} = x_2 + bo.u(t) \\ \dot{x_2} = \dot{f}(x_1, d(t), t) \\ y = x_1 \end{cases} \quad (35)$$

In matrix form:

$$\begin{cases} \dot{x} = A.x + B.u + D.\dot{f} \\ y = C.x \end{cases} \quad (36)$$

$$\begin{cases} \dot{\tilde{x}_2} = (A - LC).x + B.u + L.\tilde{y} \\ \tilde{y} = C.\tilde{x} \end{cases} \quad (37)$$

$L = \begin{pmatrix} \beta_1 \\ \beta_2 \end{pmatrix}$ with β_1 and β_2 are the parameters of the observer.

When the estimated value of the disturbance $\tilde{x}_2 = \tilde{f}$ is equal to the actual value of the disturbance f, the system behaves as if there were no disturbance at all. In fact, the system is controlled by a new signal, referred to by U_o, and that contains the exact value of the disturbance in order to overcome it. Equation (38) and Equation (39) are respectively the forms of the new control signal and the new system.

$$U_o = bo.u + f(t) \quad (38)$$

$$\begin{cases} \dot{x_1} = U_o \\ y = x_1 \end{cases} \quad (39)$$

The transient profile (Equation (39)) of the initial system is a simple integrator that can be easily controlled by a proportional controller chosen as follows in Equation (40), where ω_c refers to the desired natural frequency of the closed loop transfer function [16].

$$K_p = \omega_c \quad (40)$$

Also, parameters β_1 and β_2 of the matrix L need to be determined to make the observer function efficiently. For that, we use the method of pole placement combined with the ω_o*_Parametrization* suggested in [17]. It consists on assigning all eigenvalues of the observer at -ω_o. This ω_o is the bandwidth of the observer which a common rule suggest to chose it as in Equation (41) [17].

$$\omega_o = 3 \sim 5.\omega_c \quad (41)$$

Figure-4 illustrates the ADRC topology for a first order system.

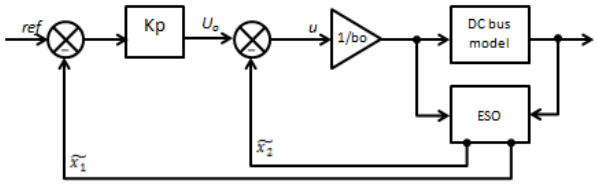

Figure-4. ADRC Topology.

Control of rotor current and grid current with ADRC

The ADRC makes it possible to see each of the rotor currents of the DFIG and each of the grid currents as an independent system by decoupling them from each other. Actually, the coupling term in the model of the system is considered as a disturbance to be overcome by the control signal thanks to the ESO. To apply the ADRC in the control of the currents, we need to put them in the form given in Equation (35) using Equation (14), (15), and (22). The results are given in Equation (42), (43), (44), and (45).

$$\begin{cases} \dot{x_1} = \dot{\iota_{rd}} = x_2 + bo_{rd}.V_{rd} \\ \dot{x_2} = \dot{f_{\iota_{rd}}}(i_{rd}, i_{rq}, V_{rd}, t) \\ y = x_1 \end{cases} \quad (42)$$

$$\begin{cases} \dot{x_1} = \dot{\iota_{rq}} = x_2 + bo_{rq}.V_{rq} \\ \dot{x_2} = \dot{f_{\iota_{rq}}}(i_{rq}, i_{rd}, V_{rq}, t) \\ y = x_1 \end{cases} \quad (43)$$

$$\begin{cases} \dot{x_1} = \dot{\iota_{fd}} = x_2 + bo_{fd}.V_{fd} \\ \dot{x_2} = \dot{f_{\iota_{fd}}}(i_{fd}, i_{fq}, V_{fd}, t) \\ y = x_1 \end{cases} \quad (44)$$

$$\begin{cases} \dot{x_1} = \dot{\iota_{fq}} = x_2 + bo_{fq}.V_{fq} \\ \dot{x_2} = \dot{f_{\iota_{fq}}}(i_{fq}, i_{fd}, V_{fq}, t) \quad \text{t} \\ y = x_1 \end{cases} \quad (45)$$

with:

$$f_{i_{rd}} = \omega_r.i_{rq} - \frac{R_r}{L_r - \frac{M^2}{L_s}}.i_{rd} + \Delta bo_{rd}.V_{rd}$$

$$f_{i_{rq}} = -\omega_r.i_{rd} - \frac{R_r}{L_r - \frac{M^2}{L_s}}.i_{rq} + \Delta bo_{rq}.V_{rq} - \frac{\omega_r.M.V_s}{\omega_s.L_s.\left(L_r - \frac{M^2}{L_s}\right)}$$

$$f_{i_{fd}} = \frac{-e_d}{L_f} + \omega_s.i_{fq} - \frac{R_f}{L_f}.i_{fd} + \Delta bo_{fd}.V_{fd}$$

$$f_{i_{fq}} = \frac{-e_q}{L_f} - \omega_s.i_{fd} - \frac{R_f}{L_f}.i_{fq} + \Delta bo_{fq}.V_{fq}$$

$$bo_{rd} = bo_{rq} = \frac{1}{L_r - \frac{M^2}{L_s}}$$

$$bo_{fd} = bo_{fq} = \frac{1}{L_f}$$

$f_{i_{r/f,d/q}}$ present the total disturbances affecting $i_{r/f,d/q}$,

DC bus voltage regulation with ADRC

Using the energy (W) stored in the DC capacitor as the state variable of the system, and previous Equation (23) and (25), we can put the system as follows:

$$\frac{dW}{dt} = V_q.i_q - P_m \quad (46)$$

This new system can be easily put in the form given in (35) as in Equation (47) in order to apply the ADRC method.

$$\begin{cases} \dot{x_1} = \dot{W} = x_2 + bo_{dc}.i_q \\ \dot{x_2} = \dot{f_{dc}}(W, P_m, q, t) \\ y = x_1 \end{cases} \quad (47)$$

with:

$f_{dc} = P_m + \Delta bo_{dc}.\, i_q$

$bo_{dc} = V_q$

The following Figure illustrates the control of the DC voltage by ADRC.

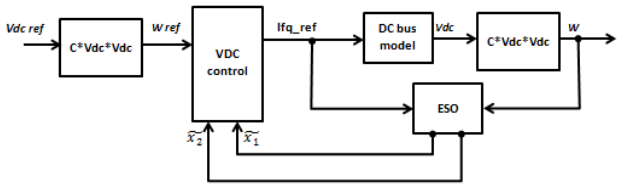

Figure-5. Control loop of the DC voltage with ADRC.

SIMULATION RESULTS

Using Matlab/Simulink for simulation, the system response when controlled by PI controllers is compared with its response when controlled by ADRC controllers. This comparison is done in terms of reference tracking and robustness.

All equations used in previous section are in receiver convention. All figures and simulations in the present section doesn't present the transition periods and start up of the wind system, and skips directly to steady state.

Reference tracking

Rotor direct and quadratic currents:

In this test, the wind speed fluctuates between 11.5 m.s^{-1} and 8.5 m.s^{-1} as in Figure-6, causing the generator speed and the electromagnetic torque reference to change.

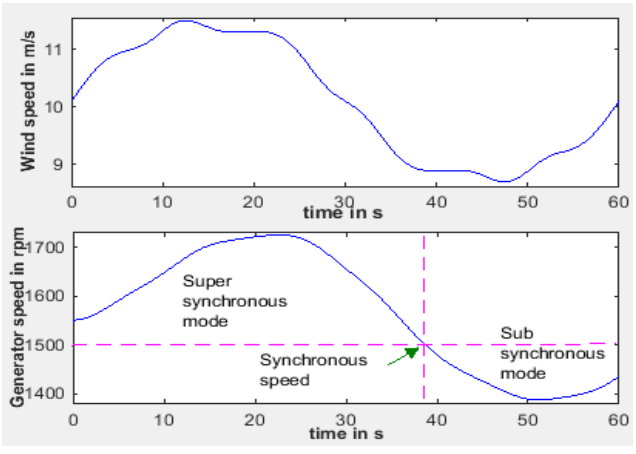

Figure-6. Wind speed in m/s and Generator speed in rpm.

The maximum power point tracking algorithm imposes a reference value of the electromagnetic torque and so imposes a reference value of the rotor quadratic current. The rotor direct current is imposed by the reference value of the reactive power. In the present test, this later value is kept null to drive the power factor to unity (1). Figures 7 and 8 present the PI controller and the ADRC ability to drive i_{rq} and i_{rd} to their references.

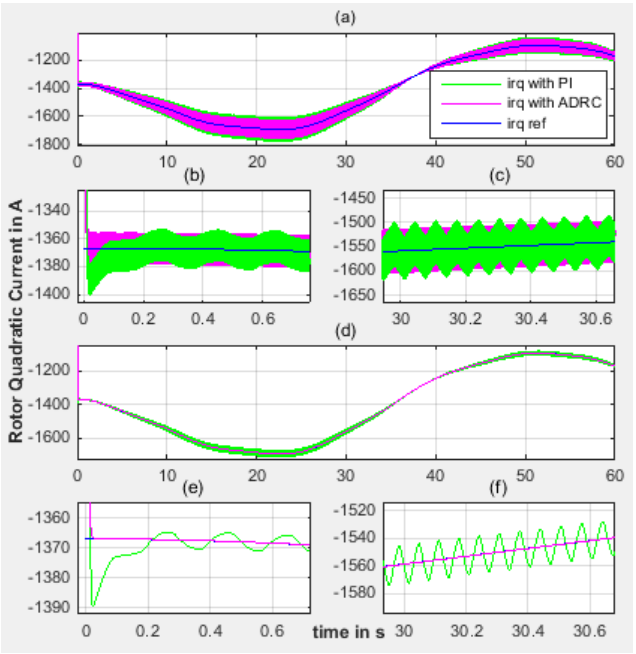

Figure-7. (a). Rotor quadratic current and its reference; (b). zoom in on Figure-7(a) at time t=0s; (c). zoom in on Figure-7(a) at time t=30s, (d). Mean value of rotor quadratic current; (e). zoom in on Figure-7(d) at time t=0s; (f). zoom in on Figure-7(d) at time t=30s.

Figures-7(a) shows that rotor quadratic current reference curve is similar to the wind and generator speed curves. As for the controllers, i_{rq} with PI control (green) falls by 1.8% of its rated value for 100ms, but with ADRC (magenta), i_{rq} follows its reference (blue) after 35ms. Previous comments are clearer with curves of mean values. Figure-7 (d) presents the mean values of i_{rq} with each of the controllers and its reference. Zoom in on the curves (Figure-7 (e) and Figure-7 (f)) shows that the mean value of i_{rq} with ADRC and i_{rq_ref} are confounded while the mean value of i_{rq} with PI also falls by 1.5% of its reference and starts fluctuating after 100ms by at least 1% (Figure-5 (d)) around the reference.

With reactive power driven to a null value, the direct rotor current reference is 100A. Figure-8 (a), (b) and (c) don't show a much difference between both controllers. However, with the mean values presented in Figure-8. (d) and the zoom in Figure-8.(e) and (f), we can notice that ADRC is quicker than PI in driving i_{rd} to its reference. It also shows that $< i_{rd} >$ with ADRC and its reference are confounded while $< i_{rd} >$ with PI still fluctuates by at least 1.5% around the reference value.

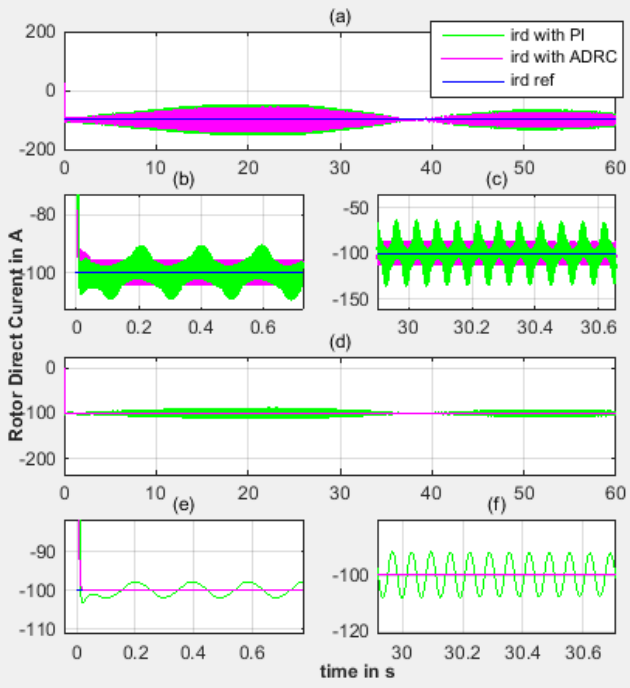

Figure-8. (a). Rotor direct current and its reference; (b). zoom in on Figure-8(a) at time t=0s; (c). zoom in on Figure-8(a) at time t=30s; (d). Mean value of rotor direct current; (e). zoom in on Figure-8(d) at time t=0s; (f). zoom in on Figure-8(d) at time t=30s.

From previous Figure-7 and Figure-8, we see that with both controllers, the direct and quadratic current are both fluctuant. This is due to the fact that rotor direct and quadratic voltages feeding the rotor of the DFIG are obtained from the PWM rotor side converter. As a result, it's more meaningful to compare the mean values $< i_{rd} >$ and $< i_{rq} >$ rather than compare their initial values.

Both these mean values are confounded with their references when control is done by ADRC and fluctuates by 1.5% around the reference when control is done by PI. Also, at t=0s, the currents don't fall far from their references with ADRC and reaches them after the desired time response. But with the PI, it took the quadratic current trice the time response to reach the reference.

All above comparison resulted in that ADRC is quicker and more suitable than the PI controller for the control of rotor currents in terms of reference tracking.

DC voltage regulation and control of filter current

To connect the rotor to the power grid, the AC voltage after the grid side converter and the filter should be fixed to the nominal voltage value of the grid that is why the voltage in the DC link should be kept at a steady value suitable to insure connection to the grid. For grid voltage value of 690V, DC voltage should be 1400V.

The following fig.9 presents the DC voltage and its reference with both PI and ADRC.

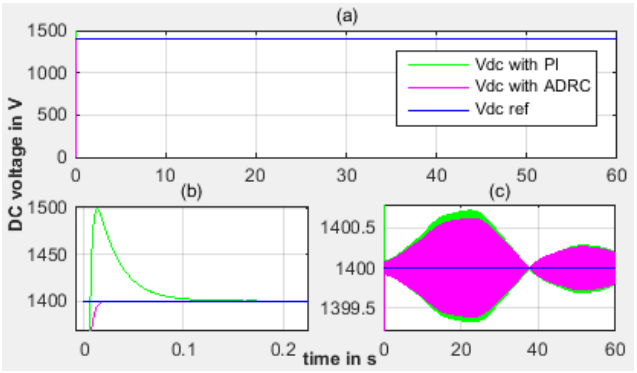

Figure-9. (a). DC voltage and its reference; (b). zoom in on Figure-9.(a) at time t=0s; (c). vertical zoom in on Figure-9(a).

Figure-9(c) shows that both controllers are efficient because the fluctuations around the V_{dc_ref} doesn't reach 1V ($\approx 0.035\%$). But the zoom presented in Figure-.(b). shows a peak DC voltage with the PI controller for about 7.1%. To evaluate the impact of this peak value, it's important to examine the filter quadratic current.

The DC bus voltage depends on the current flowing to and from the DC link. But since the rotor current are imposed by the MPPT, it's up to the filter current to regulate the DC voltage to its reference. Therefore the DC voltage regulation loop provides the system with the reference of the quadratic current in the filter (i_{qf}). Figure 10 presents i_{qf_ref} with each of the controller PI and ADRC.

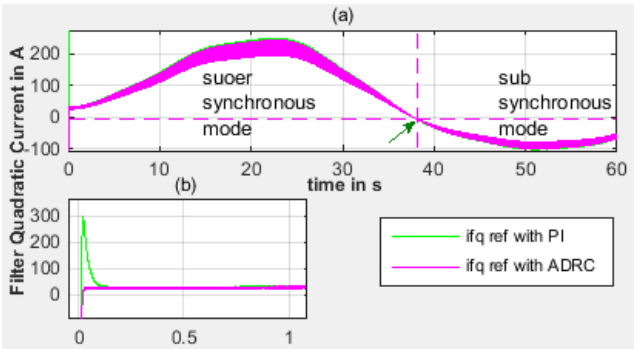

Figure-10. (a). Filter quadratic current; (b). zoom on Figure-8(a) at time t=0s.

At first sight and from the figure above, it's shown that the filter quadratic current reference with both controllers are confounded. It changes the sign when the turbine goes from supersynchronous mode to subsynchronous mode. This is contingent with the fact that the current flows from the grid to the wind turbine during subsynchronous mode and from the rotor to the grid during the super synchronous mode. This means that both controllers are well synthesized.

However, with a zoom at t=0s, it's clear that the i_{qf_ref} with PI presents a peak value of 1000% (10 times) of the reference with ADRC. This is due to the peak value

of 7.1% in the DC voltage controlled by the PI controller at time t=0s. Also, fig.11.(c) shows that the mean value of i_{qf_ref} with ADRC is steadier than with the PI.

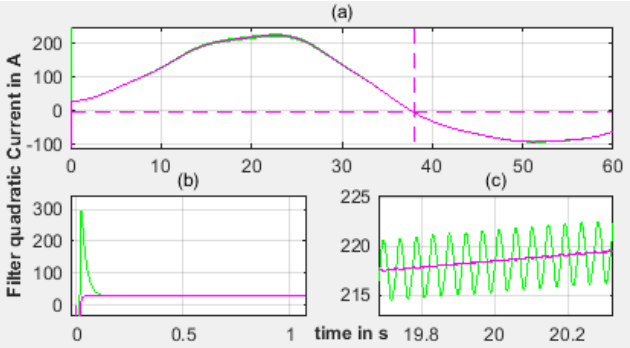

Figure-11. (a). Mean value of filter quadratic current; (b). zoom at time t=0s; (c). zoom at time t=20s.

The next Figure presents the filter quadratic current and the mean value of its reference with both controllers.

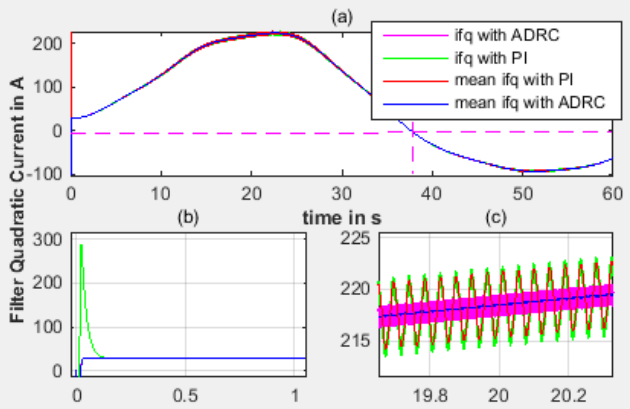

Figure-12. (a). Mean value of the reference of filter quadratic current with ADRC (blue), with PI (red), mean value of filter quadratic current with ADRC (magenta), with PI (green); (b). zoom in at time t=0s, (c). zoom in at time t=20s.

Previous Figure-12 shows that the filter quadratic current follows its reference and presents a peak value at time t=0s confounded with the peak value of its reference (Figure-12. (b)). Also, it shows from Figure-12(c) that i_{qf} with ADRC is steadier than i_{qf} with PI.

To sum up, Figure-9, Figure-10, Figure-11, and Figure-12 shows that the PI controller causes a peak value in the DC voltage and affects the reference of the quadratic filter current. This slows the system and increases its time response. But with the ADRC control, both the DC voltage and the filter current don't exceed their references and reach them at the desired time response. Moreover, we can say that the realistic value of i_{qf_ref} is the one obtained with ADRC. So, if we compare the i_{qf_ref} of ADRC with i_{qf} of PI (Figure-12.(b)), it will seem that the system took 200ms to reach the reference.

Robustness test

To evaluate the robustness of each of the controller, we simulate the system with a change in the internal variables of the generator and compare the rotor currents before and after the parametric variation. To do so, we spare the system the fluctuating character of the rotor voltages due to the rotor side converter, and we feed the generator model by the exact reference value of voltages obtained from the control loop of the current. Figures 13 and 14 shows respectively the rotor quadratic and direct currents with each of the controllers when the rotor resistance becomes twice its initial value. Also, figures 15 and 16 shows respectively the rotor quadratic and direct currents with each of the controllers when the inductions of the system becomes twice their initial values.

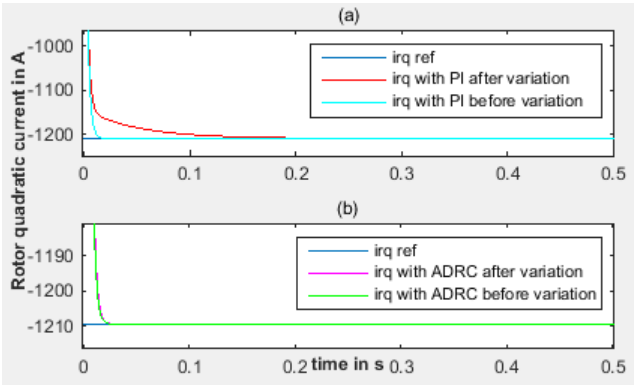

Figure-13. (a). Rotor quadratic current with the PI controller before and after R_r doubles; (b). Rotor quadratic current with ADRC before and after R_r doubles.

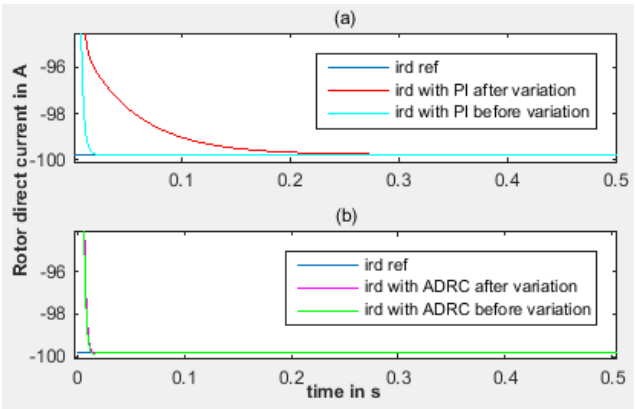

Figure-14. (a). Rotor direct current with the PI controller before and after R_r doubles; (b). Rotor direct current with ADRC before and after R_r doubles.

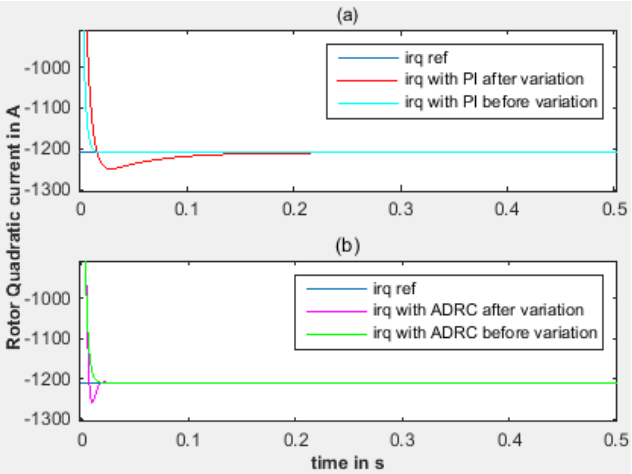

Figure-15. (a). Rotor quadratic current with the PI controller before and after R_r doubles; (b). Rotor quadratic current with ADRC before and after the inductions double.

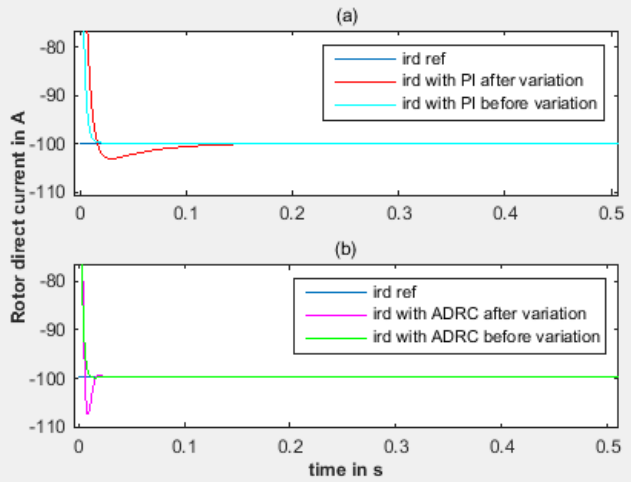

Figure-16. (a). Rotor direct current with the PI controller before and after the inductions doubles; (b). Rotor direct current with ADRC before and after the inductions double.

We deduce from the last four figures that the PI is the most affected by modeling errors manifested in parametric variations. For instance, when the rotor resistance doubles, the integral gain, which is function ofR_r, becomes inappropriate. Same for the proportional gain when the inductions double.

However, when any of the previous variables changes, the term $\frac{K_i}{K_p}$ is no longer compensating the pole of the open loop transfer function [9] and the time response of the system is no longer equal to $\frac{\left(L_r-\frac{M^2}{L_s}\right)}{K_p}$. Therefore, not only one parameter of the PI becomes inappropriate but also the other, causing the time response of the controlled system to be far from the desired value.

As for the ADRC, despite of the exceeding presented in Figure-15 (b) and Figure-16 (b), it still is the least affected by the variations and even when it does, the system still joins its reference after the exact desired time response.

CONCLUSIONS

Tow controllers have been compared in this paper. The first is the classic PI controller and the second is a method suggested by Chinese Prof. Han and named the active disturbance rejection controller. Both controllers were used in the different control loops in a wind system based on famous doubly fed induction generator and compared in terms of reference tracking and robustness against parametric variations.

To parameterize the controller, two methods are used for the PI such as the pole compensation the fixed gain margin. As for the ADRC, it was presented and developed as first suggested by its creator. It's mainly based on the extension of the system by one more additional variable containing all disturbances affecting the system and estimated by an extended state observer.

Both methods proved their ability to drive the system variables to their references, respecting the changes in the functioning of the system when it goes from subsynchronous to supersynchronous mode. However, the comparison showed that ADRC is less sensitive to parametric variation that occurs due to modeling errors or external conditions such as the increase of the temperature. Also, ADRC proved its ability to drive the system to its reference at the desired time of response unlike the PI controller. This later controller presented delays in the response and exceeding of the reference in many of the tests presented in this paper.

REFERENCES

[1] Bhattacharya *et al.* COP21 at Paris: What to expect, the issues, the actors, and the road ahead on climate change. Global economy and development at Brookings, www.brookings.edu.

[2] Zineb Mouline. COP21, from a Moroccan Perspective. http://www.nitech.ac.jp.

[3] M. Liserre, R. Cardenas, M. Molinas, and J. Rodri´guez. 2011. Overview of multi-MW wind turbines and wind parks. IEEE Trans. Ind. Electron. 58(4): 1081-1095.

[4] Yaramasu V.; Bin Wu; Sen, P.C.; Kouro, S.; Narimani, M. 2015. High-power wind energy conversion systems: State-of-the-art and emerging technologies. in Proceedings of the IEEE. 103(5): 740-788.

[5] R. Mukand Patel. 1999. Wind and solar power system. CRC press.

[6] A. Betz. 1986. Wind energy and its utilization by windmills. Windenergie und ihre Ausnutzung durch

Windmühlen. (in German), Vandenhoek und Rupprecht, Göttingen.

[7] M. Stiebler. 2008. 'Wind energy systems for electric power generation. Green energy and technology, Springer-Verlag, berlin, Heidelberg.

[8] S. El Aimani. 2004. Modélisation de différentes technologie d'éoliennes intégrées dans un réseau de moyenne tension. Thèse de doctorat, Université des Sciences et Technologie de Lille.

[9] F. Poitiers. 2003. Etude et commande de génératrices asynchrones pour l'utilisation de l'énergie éolienne. Université de Nantes.

[10] Guy Séguier. 1999. Electronique de puissance: Les fonctions de base et leurs principales applications. 7ème édition, Dunod, Paris.

[11] R. Pena, J. C Clare, and G. M. Asher. 1996. Double fed induction generator using back to back PWM converters and its application to variable speed wind-energy generation. IEE roc. -Electr. Power Appl. 143(3): 231-241.

[12] Sylvain Lechat Sanjuan. 2010. Voltage oriented control of three-phase boost WM Converters, Master of Science thesis in electric power engineering. Chalmers University of Technology, Goteborg, Sweden.

[13] Papanicola Robert, Course. Précision des Systèmes Asservis. Sciences Industrielles.

[14] Han, Jingqing. 2006. From PID to active disturbance rejection control. IEEE transaction on industrial electronics. 21(2).

[15] R. Chakib, A. Essadki, M. Cherkaoui. 2014. Active disturbance rejection control for wind system based on a DFIG. International Journal of electrical, computer, Energetic, Electronic and Communication Engineering. 8(8).

[16] A. Boukhriss, T. Nasser and A. Essadki. 2013. A Linear Active Disturbance Rejection Control applied for DFIG based Wind Energy Conversion System. IJCSI International Journal of Computer Science Issues. 10(Issue 2, No 2).

[17] Zhiqiang Gao. 2003. Scaling and bandwidth-parameterization based controller tuning. in American Control Conference, Proceedings of the 2003. vol. 6, no., pp. 4989-4996.

APPENDIX

DFIG

Parameter	Value
Rated power	$1.5\ MW$
Pole pairs	2
Rotor resistance $\boldsymbol{R_r}$	$8.28e-3\ \Omega$
Stator resistance $\boldsymbol{R_s}$	$10.3e-3\ \Omega$
Mutual inductance $\boldsymbol{M}$	$26.96e-3\ H$
Stator inductance $\boldsymbol{L_s}$	$26.96e^{-3} + 280.1e^{-6}\ H$
Rotor inductance $\boldsymbol{L_r}$	$26.96e^{-3} + 117.7e^{-6} H$

Turbine

Gearbox gain $\boldsymbol{G}$	$\mathbf{70}$
Moment of inertia $\boldsymbol{J}$	$1000\ kg.m^2$
Viscous friction coefficient $\boldsymbol{C_f}$	0.0024
Length of one blades $\boldsymbol{R}$	35.25 m
Air density $\boldsymbol{\rho}$	$1.225\ kg/m^2$

Filter and DC bus

DC capacitor	$\mathbf{50e^{-3}\ F}$
Filter $\boldsymbol{L_f}$ and $\boldsymbol{R_f}$	$0.25e^{-3}H$, $0.785e^{-3}\ \Omega$

Desired closed loop frequencies ω_c

Rotor currents	$\mathbf{400\ rad/s}$
DC bus	$400\ rad/s$
Filter currents	$600\ rad/s$